UEA Physics – PHY-6004Y-19 Physics Project

Investigation into advanced characterisation methods to analyse performance of multi-junction photovoltaic cells

(May 13th, 2020)

Abstract

The performance of a photovoltaic cell, particularly a multi-junction cell, is affected by the quality of its material and defects that have gone undetected in production. Undetected defects prevent cells from reaching theoretical efficiencies in practice and as a result, various methods exist for analysis. The most commonly practiced technique is I-V characterisation. When produced, the I-V characteristic can be used to extract several parameters, namely the efficiency, open-circuit voltage (V_{OC}), short-circuit current (I_{SC}), maximum power output, fill-factor and shunt & series resistance. Loss mechanisms invisible to the naked eye can be identified with photoluminescence and electroluminescence imaging. As well as experimental techniques, simulation can calculate maximum efficiencies and photovoltaic cell optimisation. This research aims to investigate combinations of advanced characterisation methods that could result in precise identification of losses and develop cell technology through optimisation. A detailed breakdown of I-V characterisation of both a crystalline single-junction cell, and a triple-junction gallium arsenide cell under solar illumination is shown; these results present experimentally obtained efficiencies of 15.2%, and 26.9% respectively. Furthermore, the methodology for producing a 3D model for both a single-junction and multi-junction cell is also presented. I-V characterisation is carried out for extracting the parameters of a $1.52 \times 10^{-3} m^2$ silicon crystalline cell and a $4 \times 10^{-4} m^2$ gallium arsenide triple-junction photovoltaic cell in order to validate the model. The simulation does not provide a confirmation of experimental data as it produced anomalous results and was due to inaccurate representation of parameters within the simulation when reproducing the physical cell.

Keywords: Multi-junction solar cell; I-V characterisation; photoluminescence imaging; electroluminescence imaging; SPICE modelling

Acknowledgements

I would like to thank Dr. Kaplani for guiding me throughout the progress of the project and show gratitude for producing a learning environment that was both challenging and gratifying.

I would also like to show my gratitude to my family and friends whose continued support has empowered me to cultivate my skills as a physicist during my time at the University of East Anglia.

1. Introduction

1.1 Rationale

The motivation for the project was to produce an advanced characterisation method for multi-junction photovoltaic (solar) cells. This method would consist of several other established characterisation methods namely I-V characterisation, photoluminescence, electroluminescence and SPICE modelling. Combining these methods will capitalise on the fact that each method identifies specific faults that are not identifiable by the others. Development of solar energy aims to address the energy production aspect of the current global climate crisis.

1.2 Aims & Objectives

Due to Covid-19 different experimentation was carried out which consisted of I-V characterisation of entire cells and SPICE simulation. As a result, the new aim was to create a 3D model of a multi-junction solar cell on SPICE and to simulate the performance of a multi-junction solar cell for different scenarios of material parameters and series resistances. The hypothesis was that a combination of methods would result in accurate identification of losses and in turn improve performance through optimisation.

1.3 Methodology

The methodology consisted of producing I-V characteristics of both single and multi-junction photovoltaic cells at 25°C and 1000W/m^2 by recording the current after sweeping across a given voltage of 0V-3V. This data was imported to MATLAB using the relevant .csv files and plotted. As a result, the technical specifications of the cells were extracted. In addition, 3D models of solar cells were produced in LTSpice and simulated to produce I-V characteristics using methods utilised in Steiner et al., (2011) and Steiner et al., (2012). The results of the simulations were then compared to experimentally obtained data.

1.4 Outline

As a summary, Section 2 will discuss the theoretical background that was researched throughout the duration of the project. Furthermore, Section 3 addresses how the methodology was designed, and what the intentions and expectations were for the results. Subsequently, Section 4 will present the findings of the experimentation and present the various forms of data that were produced through the various characterisation techniques described in Section 1. Additionally, Section 5 will discuss the possible interpretations of the data and whether the overall aim was achieved; also, the papers that guided the direction of the project will be referenced to further interpret the results and determine the accuracy and any benefits from the implemented methodology. Finally, Section 6 will summarise the findings of the project, establish whether it can be implemented further and determine what future projects and papers can take away from this.

2. Literature Review & Background

2.1.1 Photovoltaic Effect

In order to appreciate the importance of producing an overall characterisation of a photovoltaic cell, it is important to get a grasp of the fundamentals. Photovoltaic or solar cells are electrical devices that convert the energy from light into electrical energy using the photovoltaic effect.

The photovoltaic effect can be likened to the photoelectric effect where instead of ejecting electrons, incident light on homogeneous material produces excess charge carriers, namely electron-hole pairs. Homogeneous material is uniform and cannot be mechanically broken down into other materials. When this effect occurs, almost all the energy from the incident light is converted into heat through non-radiative recombination where the annihilation of an electron-hole pair occurs.

2.1.2 Bandgap

Another important idea within the photovoltaic effect is the different energy levels that an electron can occupy within an atom, these are referred to as energy bands. The valence band is determined by the energy of the electrons that occupy the outermost shell of the atom. Through excitation, the valence electrons can then be excited into the conduction band. These bands carry a lot of weight for the different effects that are seen within different materials such as insulators, conductors and semi-conductors. Specifically, the bandgap is the energy difference between the highest energy state of the valence band and the lowest energy state of the conduction band as seen in Figure 1 (Hanania et al., 2018). A bandgap of a material determines the property of conductivity. When a material possesses a large bandgap, this means that the electron requires a large amount of energy to be excited from the valence band to the conduction band. These conduction electrons are what allow for the flow of current as when they are excited, they can move freely within the material and carry charge. Semiconductors have a bandgap that has a separation, but with enough energy, electrons can move into the conduction band which is an important quality for generating current without short-circuiting. Figure 2 (Semiconductor Basics, 2020) illustrates how the energy levels correspond to the structure of the atom.

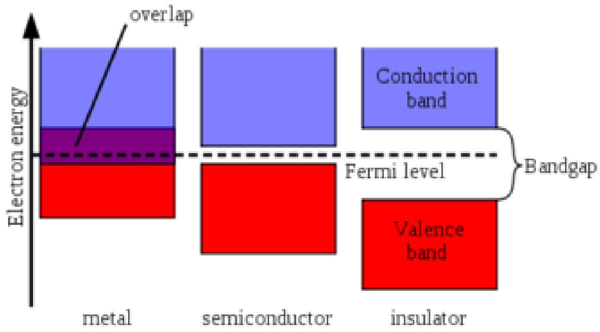

Figure 1: Diagram illustrating the bands of an electron and bandgaps for different materials [1].

2.1.3 Semiconductor

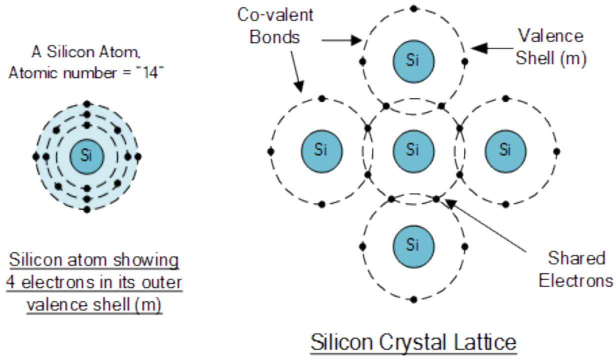

Figure 2: Diagram showing the electron orbitals of silicon [2].

Exciting the semiconductor material leads to the generation of electron-hole pairs through the combination of doping and utilisation of N-type and P-type semiconductor. As they are, semiconductors such as silicon, germanium and gallium arsenide have very few free electrons as they are packed in a crystal lattice.

To produce an N-type semiconductor, donor atoms which are classed as impurities are introduced to the silicon such as phosphorous, arsenic or antimony (shown in Figure 3, Semiconductor Basics, 2020). Four out of the five outer electrons bond with its neighbouring silicon atoms leaving one free electron to flow when current is applied. The resulting semiconductor N-type material has more electrons than holes. The electrons are thus called majority carriers while the holes are called minority carriers.

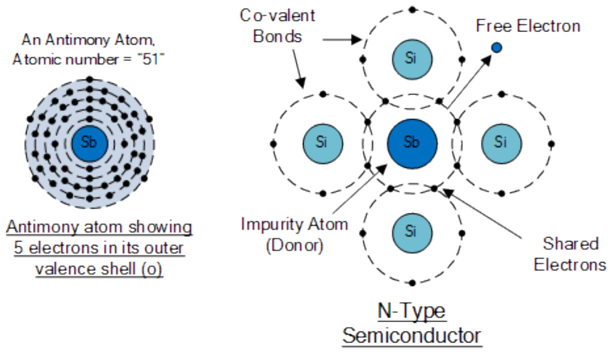

Figure 3: Diagram showing an N-type silicon doped with antimony [2].

To produce a P-type semiconductor, a trivalent impurity can be introduced to the silicon crystal lattice. The impurity can be aluminium, boron or indium with trivalence meaning they have three electrons in their outer orbital as seen in Figure 4 (Semiconductor Basics, 2020). This results in a positively charged hole as the electrons in the outer shell combine for 7. The electrons will try to move into the hole but travel through the crystal structure and as a result the lattice will become a positively charged pole as it is seeking electrons. These donor atoms are known as acceptors as they generate a hole which is constantly accepting electrons. Donor atoms produce a P-type semiconductor where majority holes are majority carriers and the free electrons are minority carriers.

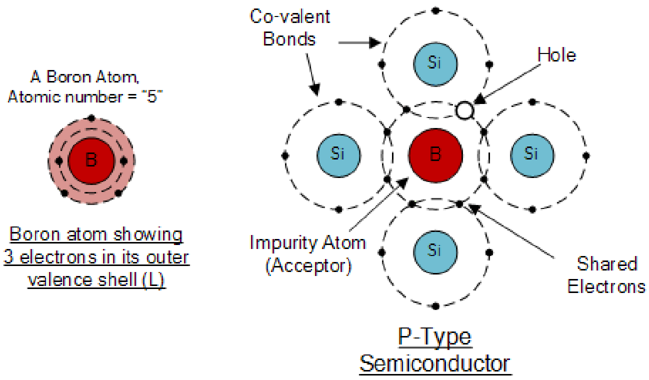

Figure 4: Diagram showing a P-type silicon doped with boron [2].

2.2.1 P-N Junction

In order to produce a potential difference using the electron-hole pairs, an inhomogeneous structure must be produced, most commonly a P-type and N-type doped semiconductor with an internal electric field known as a P-N junction.

When a semiconductor crystal is doped to form a P-N junction, some of the free electrons in the N-region begin to flow across the junction to the holes in the P-region resulting in positive ions in the N-region. As a result, the holes in the P-region flow to the N-region where there are a lot of free electrons. After this, along the junction in the P-type region there is an abundance of negatively charged ions and the area by the junction in the N-type region becomes positive. The transfer of charge consisting of holes and electrons across the P-N junction is known as diffusion. The width of the regions is determined by the extent at which each region is doped with acceptor and donor ions respectively. It will continue until the electrons which have crossed the junction have sufficient electrical energy to repel any more charge carriers from crossing the junction, setting up a potential barrier in between the two regions resulting in equilibrium. Due to the donor atoms repelling the holes and the acceptor atoms repelling the electrons, the area around the junction now becomes what is called the depletion layer as no free charge carriers can rest in a position where there is a potential barrier. The regions further away from the junction continue to have carriers. This is the reasoning for producing an inhomogeneous structure as the incident light will use the photovoltaic effect to excite electrons into the conduction band where excess charge carriers can overcome the potential barrier. A potential difference can now induce the flow of current within an external circuit and produce work in a load. Figure 5 (The P-N Junction, 2020) highlights the production of the depletion region when the P and N-type semiconductor is joined.

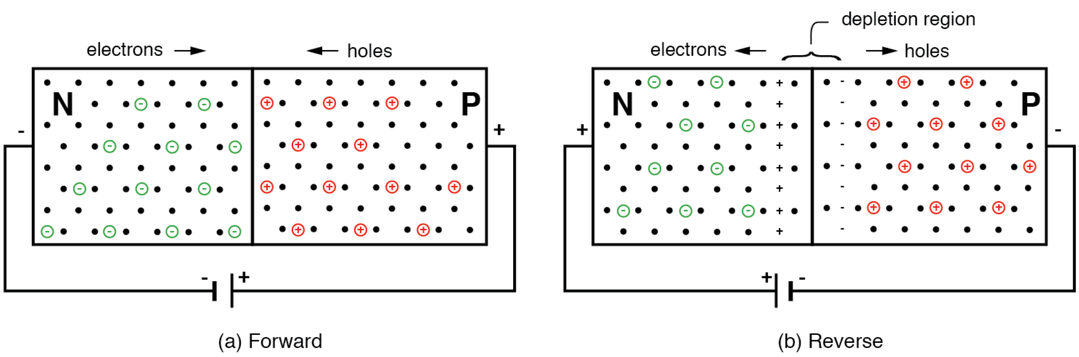

Figure 5: Diagram showing a P-N Junction [3].

2.2.2 Structure of a Photovoltaic Cell

As can be seen in the figure below (Osmanbasic, 2019), the standard two-junction photovoltaic cell does not add many more components to the standard P-N junction. Anti-reflective coating prevents photons from incident light to be reflected from the surface of the cell and contacts are added for connection to the load.

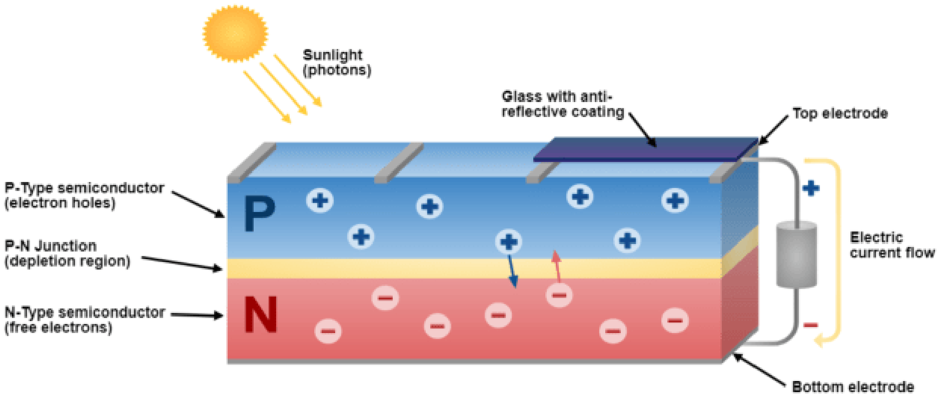

Figure 6: Diagram showing the structure of a photovoltaic cell [4].

2.2.3 Multi-junction Photovoltaic Cell

A technique that has boosted the efficiency of solar cells which multi-junction cells utilise, is stacking P-N junctions on top of each other with differing bandgaps. These differing bandgaps mean they require different energies to excite electrons into the conduction band, an important property for efficiency as the solar spectrum consists of a range of wavelengths that correspond to different energies. By stacking these materials in increasing energy level order, light that can't excite the top layer will pass through until they reach a layer which can. Figure 8 (Amyx, 2019) illustrates the idea by showing how the bandgaps spread across the wavelengths of the solar spectrum.

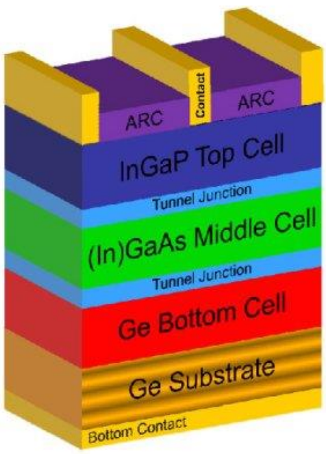

Figure 7: Schematic of multi-junction photovoltaic cell [5].

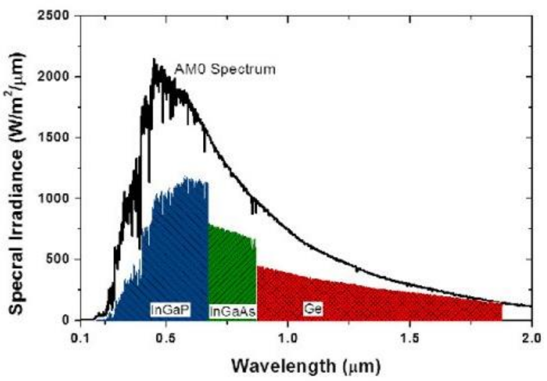

Figure 8: Diagram showing the spectral irradiance of the sun at the top of the atmosphere and the bandgaps of an InGaP/InGaAs/Ge multi-junction photovoltaic cell [5].

2.3.1 I-V Characterisation

I-V characterisation is the process of modelling the change of current as a function of the voltage of a component. In the case of a photovoltaic cell, it is carried out by using a source-meter unit and sweeping over a voltage from 0 to a given voltage and measuring the current at each point in selected intervals. The main benefits of producing an I-V characteristic is the potential of extracting selected parameters such as efficiency, open-circuit voltage and short-circuit current. Parameters that are more specific to photovoltaic cells and indicate a more detailed description such as fill-factor can also be calculated using data from the characteristic. These parameters, which can be seen in their corresponding points on the curve in Figure 9 (PVEducation, 2020), are as follows, the open-circuit voltage or V_{OC} is the maximum voltage when the cell is not connected to any circuit. The short-circuit current or I_{SC} is the current in the circuit when the cell is shorted. The maximum power output of the cell is characterised by the voltage and current at that point V_{mp} and I_{mp}. The fill-factor gives an indication of the quality of the array and is the ratio of the product of the I_{mp} & V_{mp} and the product of I_{SC} & V_{OC}. In addition, the shunt and series resistance of the solar cell can be calculated by finding the gradient of the I-V curve at the short-circuit current and the open-circuit voltage respectively. These parameters are then used in the calculation for the efficiency of the solar cell which is a measure of the power generated to the radiation power falling on it calculated by the product of the illumination and the area of the cell as shown in Equation 1 (PVEducation, 2020).

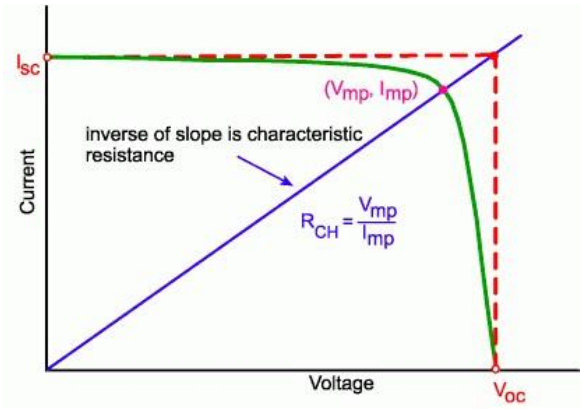

Figure 9: Graph showing an I-V characteristic and extractable parameters [6].

$$\eta = \frac{V_{mp}I_{mp}}{P_{in}} = \frac{V_{oc}I_{sc}FF}{P_{in}} \quad (1)$$

Efficiency equation for a photovoltaic cell [7].

2.3.2 Dark I-V Characteristic

Producing a dark I-V is similar to a light I-V as it produces excess carriers but instead it injects them electrically. The photovoltaic cell will ideally be in as dark conditions as possible. Although the linear plot of a dark I-V curve can illustrate how closely the cell models a diode through an exponential curve, a much more useful plot is the logarithmic plot. Figure 10 (PVEducation, 2020) shows the dark I-V curve of a photovoltaic cell with a logarithmic axis. In a lot of cases the light I-V and dark I-V are identical, but the logarithmic plot of the dark identifies the ideality of the cell by measuring the gradient at specific regions within the curve.

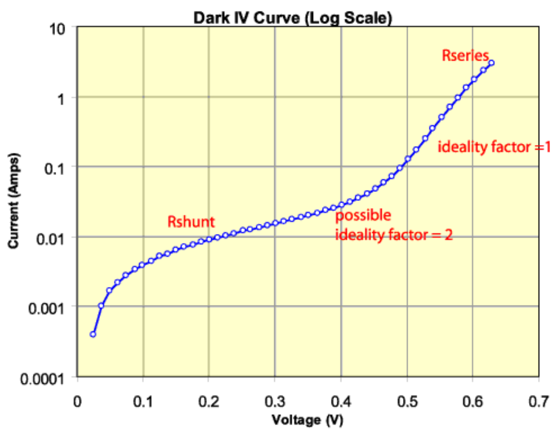

Figure 10: Logarithmic dark I-V characteristic of a photovoltaic cell [8].

2.4.1 Photoluminescence Imaging

Photoluminescence imaging is a characterisation technique that uses photoluminescence, a physical phenomenon whereby illuminated material is excited and through its relaxation emits photons. The photoluminescence can then be photographed and produces a detailed image of the structural integrity of the material as seen in Figure 11 (PV-Manufacturing, 2020). For photovoltaic cells, this is useful as physical faults within silicon often account for a large portion of the losses and can be overlooked due to the fact damages not visible to the human eye occur early in the production process. Some of these faults include shunt and series resistance issues with solar cell contacts, areas of lower diffusion lengths, iron contamination and physical defects within the silicon such as grain boundaries and dislocations. Photoluminescence imaging for multi-junction cells is more challenging as the cells consist of multiple layers which are troublesome to resolve individually. In this case several light sources must be used to illuminate specific layers and make sure that they do not excite them all. The main benefits of photoluminescence imaging come from: a short production time, non-destructive analysis and its potential for application early in the production process of the silicon as it does not require contacts.

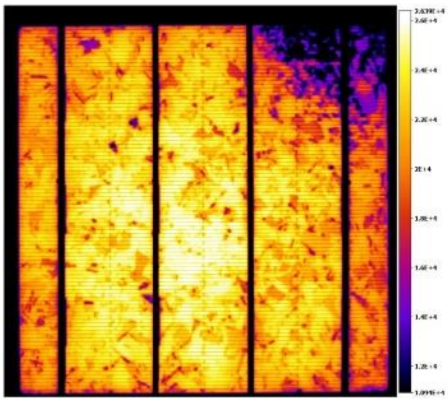

Figure 11: Photoluminescence image of a crystalline solar cell [9].

2.4.2 Electroluminescence Imaging

Similar to photoluminescence, electroluminescence makes use of another phenomenon, namely the radiative recombination from a material that is electrically charged rather than from incident light. This is due to the excitation of the material emitting photons and as a result the intensity of the regions is a function of the voltage; faulty regions show up dark which can be seen in the figure below (PVEducation, 2020). For multi-junction solar cells, it is important for subcells to be excited individually in order to resolve the individual layers as these will be the sections that will be emitting light and showing up on the image. The benefits of this form of characterisation is the short measurement time and its non-destructive characterisation. One aspect of electroluminescence that should be considered is that it requires electrical contacts. Consequently, this demonstrates it is a characterisation technique that should be utilised further along in the characterisation process.

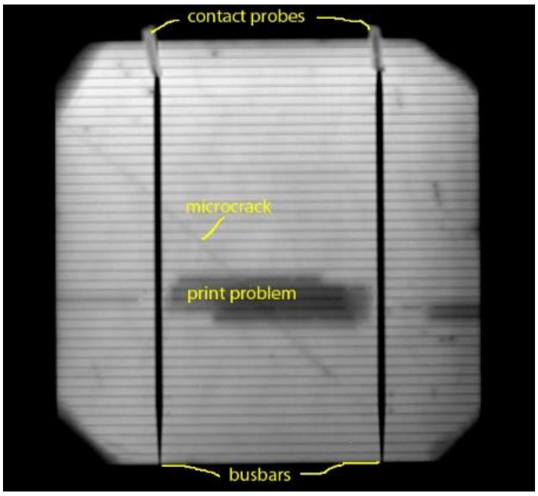

Figure 12: Electroluminescence image of silicon solar cell highlighting physical defects within the cell [10].

2.5.1 Diode Model

In order to predict and extract specific parameters of a solar cell, an equivalent electrical circuit can be constructed; this circuit is seen in Figure 13 (Characteristics of Photovoltaic Solar Cells, 2020). It is characterised by a current source that represents the photocurrent generated by the cell with a diode I_D in parallel. Since no photovoltaic cell is ideal a shunt resistance R_{SH} that represents the high conductivity paths in parallel is added. A series resistance R_S is also added which represents the various resistances in the cell originating from the fingers, busbars, metal-semiconductor contacts and base semiconductor. I_L is the current produced by the cell when connected to an external load R_L.

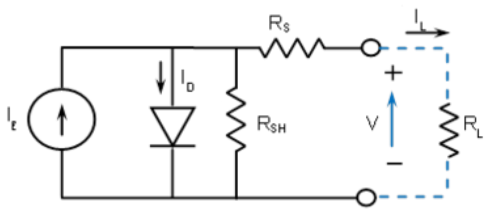

Figure 13: Equivalent electrical circuit for a solar cell [11].

2.5.2 Characteristic Equations

As stated, this model provides equations to extract parameters given experimentally obtained values. The equations for calculating the current output of the entire photovoltaic cell and diode are given below.

$$I = I_{ph} - I_D - \frac{V + Ir_s}{R_{sh}} \quad (2)$$

Equation to calculate the output current of a photovoltaic cell [12].

$$I_D = I_0(e^{\left(\frac{V+Ir_s}{mV_T}\right)} - 1) \quad (3)$$

Shockley diode equation to calculate the current flowing through the diode [12].

Equation 2 (Kaplanis, S. and Kaplani E, 2013) presents the Shockley diode equation which allows for the calculation of the current I_D flowing through the diode. I_0 is the inverse saturation current; V is the output voltage; I is the current of the photovoltaic cell; r_s is the series resistance; m is the ideality factor of the diode which is 1 when the cell is behaving ideally and 2 when recombination current is considered individually, in practice this value must be experimentally calculated. Lastly, V_T is the thermal voltage of the cell.

2.5.3 Two-diode and Three-diode Models

Using the same components and additional diodes, the model's precision can be improved by adding more diodes in parallel where they model the current I_D, the current due to pure diffusion, whilst I_r is the recombination current with I_t being the thermionic emission.

2.6 SPICE Modelling

SPICE (Simulation Program with Integrated Circuit Emphasis) is an open source program for the calculation of the operating point parameters of analog circuits. Simulation can be carried out by using one of the many SPICE programs available for use. The most commonly used program in photovoltaic modelling, particularly for 3D modelling, is LTSpice; a free-to-use software. The confirmation of theoretical models of solar cells such as the two-diode model is particularly helpful and allows for spatial resolution of the variance of performance across the length and width of the cell and even across layers such as those in multi-junction cells. 3D SPICE modelling of photovoltaic cells is based on the two-diode model and this process will be detailed in Section 3.

2.7 Placement of Report within Wider Field

The objectives of this report were influenced by several papers which have conducted research using combinations of characterisation techniques. The project intends to investigate SPICE modelling in turn to develop the process of analysing multi-junction photovoltaic cells. Throughout the research, experimentation intends to develop the practice of simulation of solar cells for confirmation of results and theoretical limits. The objectives consist of developing a 3D simulation method to quantitatively analyse the performance of multi-junction photovoltaic cells using a simulation and comparing them to experimentally obtained data.

Developing the most effective non-destructive characterisation method is the basis of this project. The efficiency and performance of photovoltaic cells is dependent on the quality of the materials in their processing and manufacture. Hoex, Zhang and Aberle, (2012) note that ‘a thorough characterisation of the individual processing steps and a detailed loss analysis of the final solar cells can be used to improve the average efficiency and yield of industrial silicon wafer solar cells.’ [16]. In particular, multi-junction photovoltaic cells consist of constituent subcells which increases the difficulty of resolving the parameters of individual layers. Lim et al., (2011) presented how ‘luminescence coupling also causes the EQE measurement artifacts in the InGaAs subcell of an InGaP/InGaAs/Ge multi-junction solar cell.’ [17]. As stated, the effects of specific characterisation methods can be seen by other techniques. Lim et al., (2011) notes ‘the methods demonstrated here can be developed into a nondestructive characterization technique for evaluating the material quality of MJ solar cells.’ [17]. Nesswetter et al., (2013) states that ‘the potential of EL imaging in combination with SPICE network simulations for multijunction cells was shown.’ [18]. These statements further highlight the importance of the amalgamation of several methods to account for the drawbacks of individual techniques and the combination of others.

Throughout the experimentation it should be noted whether these results will indicate that a combination could provide a more effective and thorough analysis of the performance of multi-junction photovoltaic cells. In addition, the method needs to provide enough quantitative evidence to have worthwhile industrial application and must produce a precise analysis of the causes of losses to be able to rectify them.

3. Method

3.1 Experimentation

3.1.1 I-V Characterisation

I-V characteristics of differing photovoltaic cells were produced over the course of a couple of weeks. For one of the experiments the solar simulator was faulty for a week, so a halogen lamp had to be used for some results. It should be noted that the efficiency parameters differ for the halogen results in comparison to the results from the solar simulator as the spectral irradiance covers a different range of wavelengths.

An important consideration is the fact that I-V curves were produced across a whole cell rather than individual subcells. Due to experimentation being cut short, details of producing an I-V curve for an entire cell will not be discussed. In order to produce an I-V characteristic, the solar simulator must be calibrated using an irradiance meter which measures the illumination that will be incident on the solar cell when it is placed in the position of the meter. Illumination is measured per square meter and is important to consider when calculating the power incident on the solar cell. Once the illumination is calibrated it is also important to calibrate the temperature of the solar cell at operating conditions as this will have an effect on the operation of the solar cell. The standard conditions were produced which were a temperature and illumination of 25°C±0.01°C and 1000W/m^2. Once achieved, the solar cell is placed at the same distance with uniform illumination and the negative contact is on the top of the cell with positive on the bottom. The source meter unit then sweeps over a range of voltages, in this case 0V to 3V with a step of 50mV and 100mV. It then records the current at these voltages and saves the data to a .csv file that was saved and imported to MATLAB to plot and extract the parameters. For a dark I-V the same process was carried out under dark illumination. The different types of I-V characteristics produced were a light and dark I-V for a crystalline silicon single-junction solar cell under both halogen and solar simulator illumination. The same was conducted for a gallium arsenide triple-junction solar cell producing a dark and light I-V. A similar set-up can be seen in Figure 14, but it does not show the solar simulator and uses a thermocouple instead. The results from this are displayed in the results section.

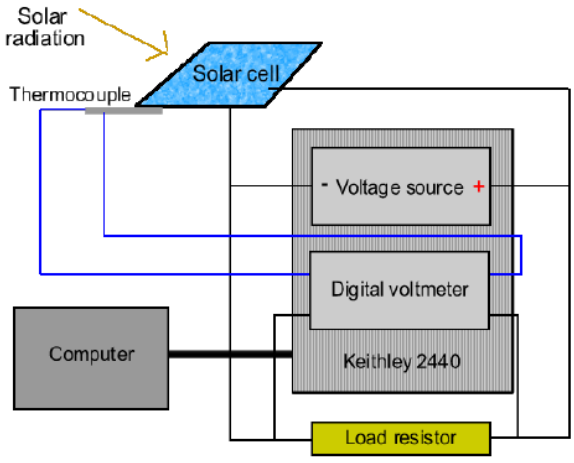

Figure 14: Analogous set-up for producing an I-V characteristic – Malik, et al. (2010).

3.1.2 SPICE Simulation

SPICE simulation initially was designed to be the final set of experimentation to confirm and match the data obtained in the other experiments, however, due to situational issues SPICE became a much larger portion of experimentation. To build up familiarization and experience with SPICE, the simulation began with producing a two-diode model of a solar cell and extracting some of the parameters with the code inside the software.

Figure 15 displays the model that was produced within LTSpice with several components depicted: I1 representing a photocurrent of 0.541A; D1 and D2 representing the diode currents of 1.0×10^{-10}A; and a series and shunt resistance possessing an ohmic resistance of 1000Ω and 0.3125Ω. The voltage source is used to sweep the voltage from 0V to 0.87V with a step of 100mV; 'model .dc V1 0 0.87 1m' represents the sweep in the commands in the image. The other commands also calculate the I_{SC}, V_{OC} and P_{Max} at operating conditions which are shown in section 4. Producing this was crucial for developing an understanding of the diode model as well as gaining proficiency with the software.

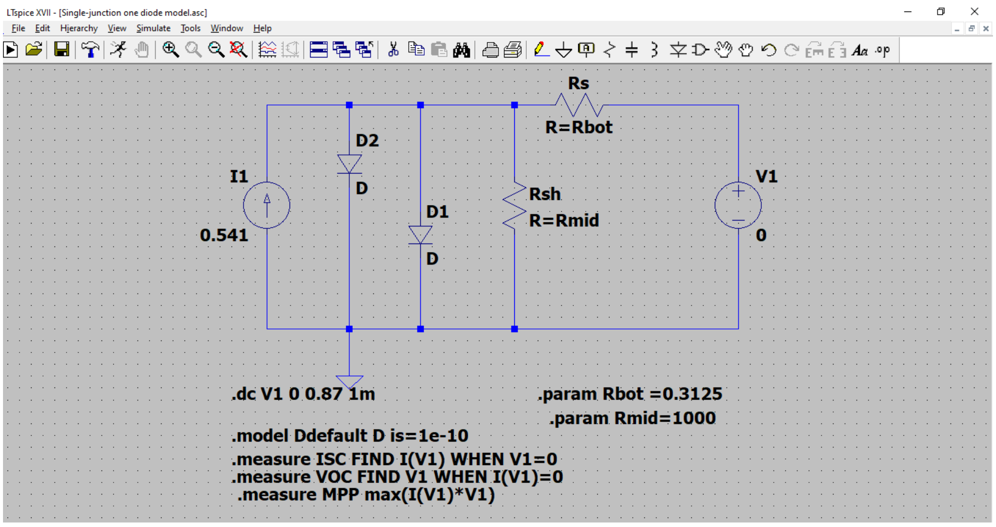

Figure 15: Screenshot within LTSpice of two-diode model.

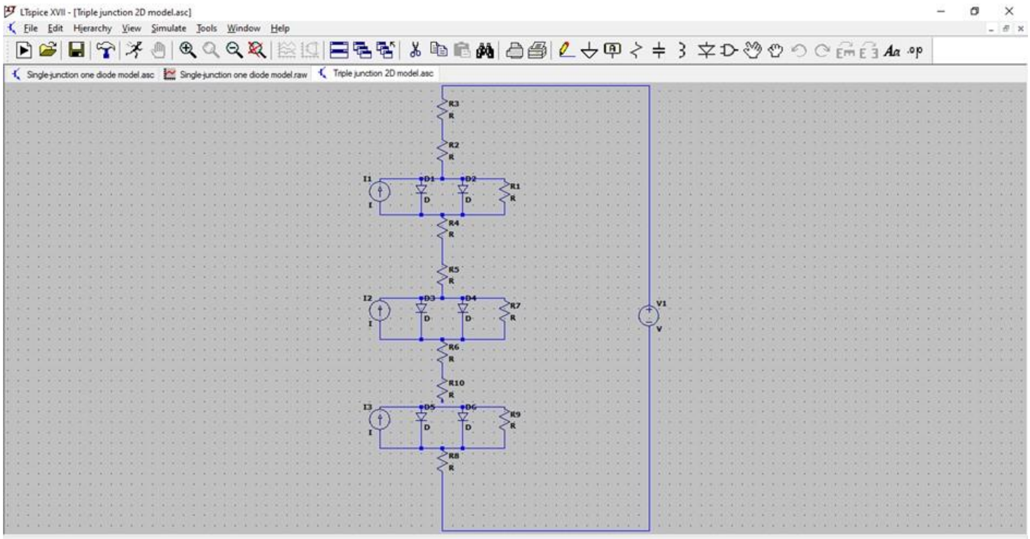

Figure 16: Triple-junction 2D model.

In order to develop this model, Ho, D. F. & Morgan, D. T. (1991) describes a method to produce a two-dimensional simulation that stacks layers of the two-diode model and wires it accordingly with equivalent resistances for the tunnel diode. The model was successfully produced; however, the paper did not include parameters as they were experimentally obtained and as it was not possible to obtain these in the laboratory, an I-V characteristic could not be produced. The process was the same as the single-junction model with resistances above and below the cells. Moreover, the method did not relate entirely to the more advanced models that allow for the spatial variation within the cell, consequently the method was ignored.

One hurdle originated from producing a model that varied spatially in three dimensions as LTSpice does not possess the settings to rotate components at 45°. As 3D modelling of analog circuits is not frequently practiced, there was little material on the subject other than within the research papers. It is understandable as there is often not a need to produce three dimensional circuits as they differ minimally across three dimensions and are not made of large 3D spatially variant material. In any case, past papers did not go into much detail about producing the three-dimensional model in terms of wiring and placing components. Wiring the components in three-dimensions is straight forward as there is a setting to wire components non-orthogonally. In order to rotate the resistor, the assumption was made that the resistor component at 45° must be an original component not within the software. This was done manually by altering the original model of the resistor within the editing tool of the software and leaving the two ends so it would still wire correctly and produce an accurate resistance value.

Currently, it is not clear if it is the correct methodology as no published information provides details of the process. The assumption relies on the idea that it should not affect the final simulation if the two pins of the resistor remain within the component in LTSpice. In order to produce a 3D model, it was important to identify the main differences between it and the 2D diode model. Steiner et al., (2011) breaks down the modelling approach and presents how the two diode-model is representative of the whole cell as well as not accounting for variation of different sections within the cell which behave differently. The 3D model accounts for this is by dividing the model into elementary cells which represent a small area of the cell and entering parameters with a current density. These areas are determined by the overall area of the cell being simulated and dividing it by the number of elementary cells within the model. Each elementary cell now represents a portion of the total area of the physical 3D model that is in the laboratory. If the cell being simulated is $1cm^2$ and the number of elementary cells is 16, then the area of one elementary cell is $625\mu m^2$. Intuitively, the greater the number of elementary cells provides a greater precision and resolution, however, the time required for simulation also increases. As well as representing a physical area within the real cell, the different regions possess different behaviours.

Figure 17 (Steiner et al., 2011) depicts the three different elementary cells in the model for a single-junction cell. The different regions represented are the dark elementary cell which is shaded by the busbar (metallic contact) of the solar cell and as a result has no generated photocurrent. The illuminated elementary cell accounts for the majority of the generated photocurrent and

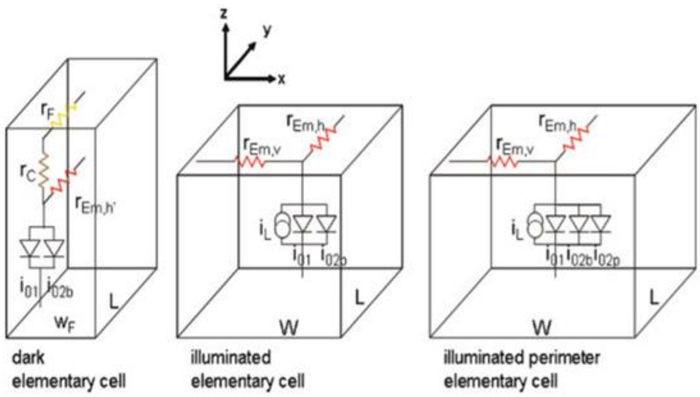

Figure 17: Elementary cells for a 3D model of a photovoltaic cell. [13]

the illuminated perimeter elementary cell. The model still contains the components from the diode-model that now possess variation across the model. The total values for the current and resistances are now the sum of the values produced by each elementary cell. As a result, the parameters of the model are densities.

Steiner et al., (2011) provides the parameters for simulation which were experimentally obtained. As experimentation was drawn to a halt, the parameters that are given within the paper were used to attempt to replicate the results.

$$i_L(x,y) = -A(x,y) \cdot C \cdot J_L(C=1) \tag{4}$$

$$i_{01}(x,y) = A(x,y) \cdot J_{01}[e^{\left(\frac{qV(x,y)}{kT}\right)} - 1] \tag{5}$$

$$i_{02b}(x,y) = A(x,y) \cdot J_{02b}[e^{\left(\frac{qV(x,y)}{2kT}\right)} - 1] \tag{6}$$

$$i_{02p}(x,y) = S(x,y) \cdot J_{02p}[e^{\left(\frac{qV(x,y)}{2kT}\right)} - 1] \tag{7}$$

$$r_{Em,v}(x,y) = \frac{r_{Em} \cdot W}{L} \tag{8}$$

$$r_{Em,h}(x,y) = \frac{r_{Em} \cdot W}{L} \tag{9}$$

$$r_F(x,y) = \frac{\rho_M \cdot L}{h_f \cdot W_F} \tag{10}$$

$$r_C(x,y) = \frac{\rho_C}{A(x,y)} \tag{11}$$

$$r_{base}(x,y) = \frac{\rho_{base} \cdot d_{base}}{A_{SZ}} \tag{12}$$

$$r_{rearcontact}(x,y) = \frac{\rho_{RC}}{A_{SZ}} \quad (13)$$

The equations presented above describe the different parameters for the respective elementary cells. i_L calculates the absolute value of the generated photocurrent for the illuminated elementary cells where *A(x,y)* is the area the elementary cell is representing and *S(x,y)* is the fraction of solar cell surrounding perimeter assigned to one J_{02p}-diode. C is the concentration ratio and $J_L(C=1)$ is the photogenerated current density at one sun. i_{01}, i_{02b} and i_{02p} are the different diode currents. J_{01}, J_{02b} and J_{02p} are the different current densities in the neutral & depletion zone and the perimeter. *V(x,y)* is the voltage across the load. T is the absolute temperature of the cell in Kelvin, q is the elementary charge 1.6×10^{-19}C and k is Boltzmann's constant which is equal to $1.38 \times 10^{-23} m^2 kg s^{-2} K^{-1}$. $r_{Em,v}$ and $r_{Em,h}$ are the series and shunt resistances of the elementary cells with W and L as the width and length of the elementary cell. The resistance of the fingers is determined by r_F and the contacts is r_C where ρ_M is the resistivity of the metallization; h_f is the height of the fingers; W_f is the width of the fingers and ρ_C is the resistivity of the contact. The resistance values of the base and rear contact are calculated by r_{base} and $r_{rearcontact}$ where ρ_{base} and ρ_{RC} are the resistivities of the base and rear contact. The thickness of the base is given by d_{base} and A_{SZ} is the total area of the entire cell.

These parameters were then input into the simulation and run. A model of the single-junction 3D model produced can be seen in Figure 18 and the I-V characteristic generated by the model can be seen in Figure 26.

For the 3D simulations, the values calculated from the equations in Steiner et al., (2011) were as follows ('lcl' denotes the different lateral conducting layers and 'bot', 'mid' and 'top' denote the different subcells):

Table 1: Summary of simulation parameters for single-junction cell

Parameter	Value
i_L (A)	-1.85×10^{-5}
$r_{Emv,h}$ (Ω)	110
r_f (Ω)	3.5×10^{-6}
r_c (Ω)	6.45×10^{-6}
r_{base} (Ω)	1.2×10^{-4}
$r_{rearcontact}$ (Ω)	3.5×10^{-2}
i_{01} (A)	4.0×10^{-20}
i_{02b} (A)	2.0×10^{-11}
i_{02p} (A)	1.0×10^{-12}

Table 2: Summary of simulation parameters for triple-junction cell

Parameter	Value
i_{Lbot} (A)	-20.8 $\times 10^{-3}$
i_{Lmid} (A)	-14.9 $\times 10^{-3}$
i_{Ltop} (A)	-14.6 $\times 10^{-3}$
r_m (Ω)	2.0×10^{-6}
r_c (Ω)	3.0×10^{-6}
r_{lcl1} (Ω)	190
r_{lcl2} (Ω)	1737
r_{lcl3} (Ω)	69
r_{lcl4} (Ω)	298
r_{lcl5} (Ω)	17
r_{bc} (Ω)	3.0×10^{-5}
i_{top} (A)	4.5×10^{-27}
i_{mid} (A)	4.0×10^{-20}
i_{bot} (A)	1.0×10^{-5}

As the project was centred around multi-junction cells, it was important to produce a simulation for a triple junction cell. Steiner et al., (2012) produces an analogous method to the single-junction model, simulating a triple-junction cell. The main differences between the two models were the presence of tunnel diodes between subcells and only consisting of two-types of elementary cells. The model was developed in the same way as the single-junction model and the parameters calculated and utilised. The model can be seen in Figure 19 with the final resulting I-V curve in Figure 27.

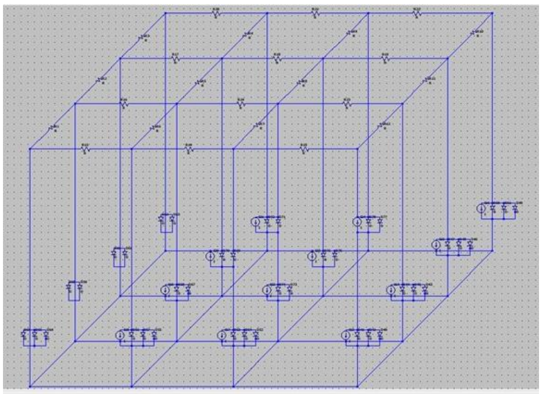

Figure 18: 3D single-junction model produced in LTSpice.

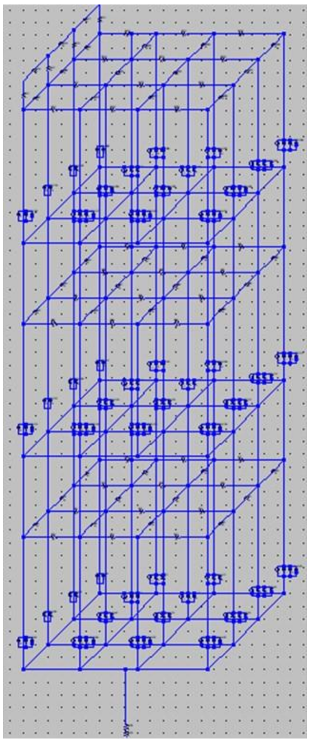

Figure 19: 3D model of a triple-junction photovoltaic cell.

4. Results

In total, two different photovoltaic cells were tested experimentally by producing their I-V characteristic; a single-junction silicon crystalline photovoltaic cell and a multi-junction germanium cell. Additionally, three LTSpice simulations were run with the results presented in the following section.

4.1 I-V Characterisation

Here are the results for the two different types of cells under differing types of illumination, namely a solar simulator and a halogen lamp. cSi (crystalline silicon) is illuminated with a halogen lamp and cSiB (crystalline silicon) and GaAs (gallium arsenide) are both illuminated with a solar simulator. The cSi cell has an area of $1.52x10^{-3}m^2 \pm 8x10^{-5}m^2$, was at a temperature of 25.1°C±0.01°C and had a voltage step of 5mV. cSi B is an identical cell to cSi and had a temperature of 25.1°C±0.01°C and a voltage step of 5mV. The triple-junction gallium-arsenide cell had an area of $4x10^{-4}m^2 \pm 4x10^{-5}m^2$ and its parameters under solar simulator illumination were extracted at a temperature of 25.04°C±0.01°C and a voltage step of 10mV. All the cells had an illumination of 1000W/m^2 resulting in a power input of 0.4W±0.041W for the GaAs cell and 1.52W±0.08W for the crystalline solar cell.

Table 3: Summary of experimentally extracted parameters from solar cells.

Parameter	Crystalline silicon /cSi	Crystalline silicon /cSiB	Gallium arsenide /GaAs
V_{OC} (V)	0.61	0.612	2.54
I_{SC} (A)	0.541	0.549	0.0507
P_M (W)	0.188	0.231	0.108
V_{MP} (V)	0.405	0.48	2.23
I_{MP} (A)	0.465	0.48	0.0482
FF	0.571	0.686	0.835
$Efficiency$ (%)	13%±1%	15%±1%	27%±1%
R_{SH} (Ω)	71.4	56.2	1230
R_S (Ω)	0.313	0.133	2.65

As most of the parameters were digitally obtained in MATLAB as points in a graph with a large resolution, the error for most of the points can be estimated to be around 1% which will be the result of having to resolve points on the line which will have a spread of around 0.01 on the x and y axis.

For comparison PVEducation [56] breaks down photovoltaic cell records for different types. The most efficient cell which is of InGaP/GaAs/InGaAs type at one-sun illumination is 35.8% with a V_{OC} of 2.62V, a J_{SC} of 14.37mAcm^{-2} and a fill-factor of 0.85. The most efficient silicon cell at one sun has been 25%, with a V_{OC} of 0.706V and a J_{SC} of 42.7mAcm^{-2} and a fill-factor of 0.828.

4.2 Light I-V

The I-V characteristic from the experiment carried out with a 1.52x10^{-3}m^2 crystalline silicon solar cell under halogen light illumination of 1000W/m^2 is shown in Figure 20 with the extracted technical specifications summarised in section 5.1. The I-V characteristics from the experimentation for the same 1.52x10^{-3}m^2 crystalline silicon cell and a 4.0x10^{-4}m^2 gallium arsenide triple-junction solar cell under solar simulator illumination of 1000W/m^2, are shown in Figure 21 and Figure 22; the results of which are summarised in section 5.1.

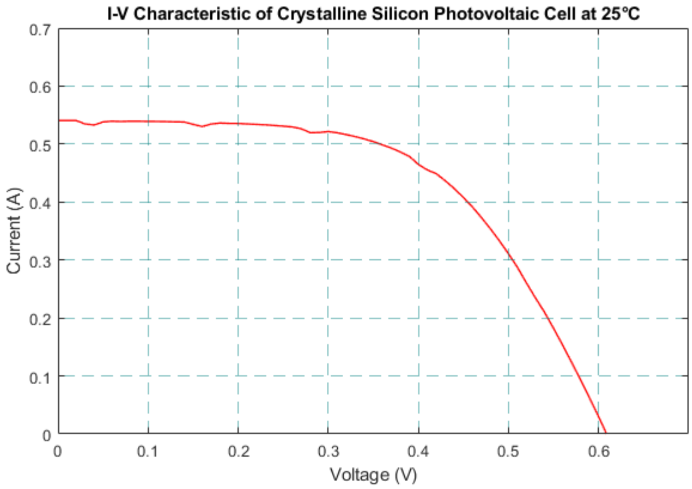

Figure 20: I-V characteristic of crystalline silicon PV cell under halogen lamp illumination of 1000W/m^2.

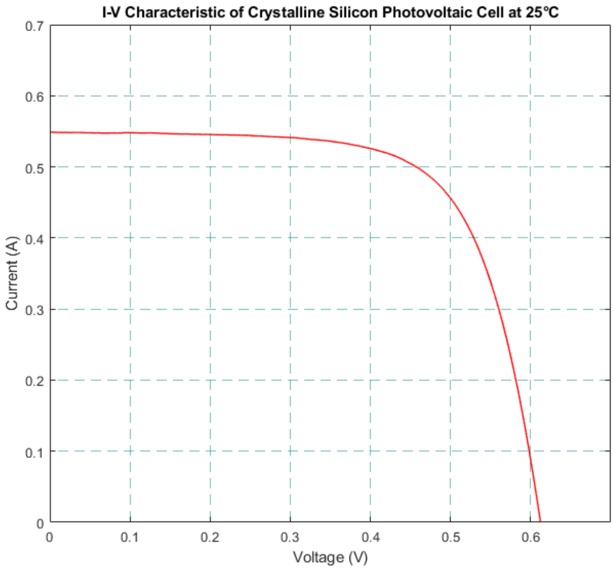

Figure 21: I-V characteristic of crystalline silicon PV cell under solar simulator illumination of 1000W/m^2.

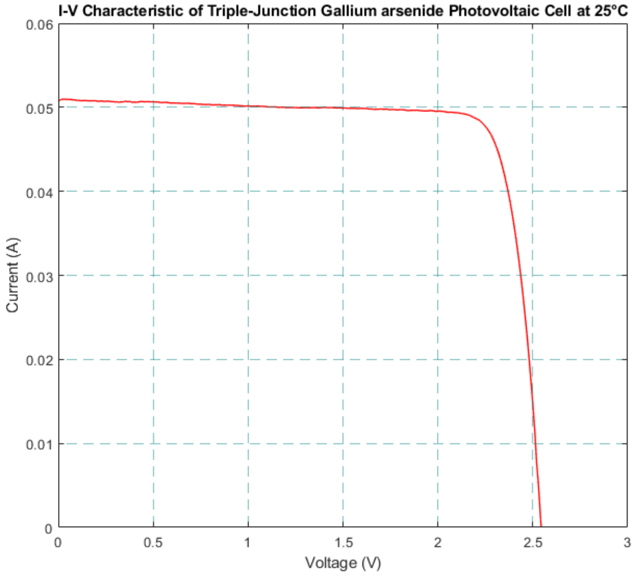

Figure 22: I-V characteristic of triple-junction PV cell under solar simulator illumination of 1000W/m^2.

4.3 Dark I-V

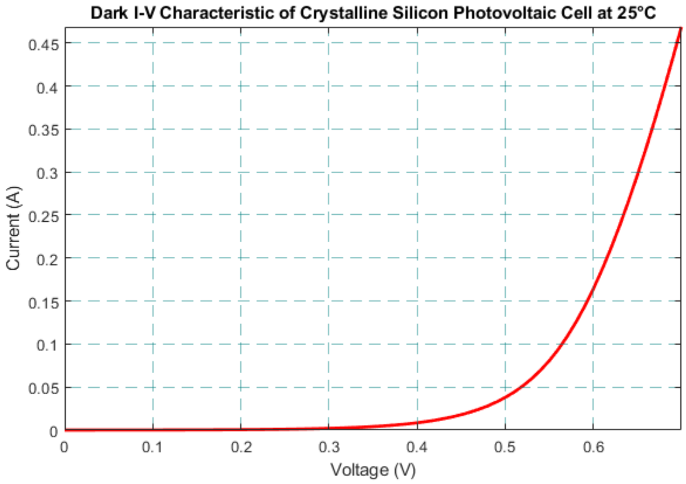

Figure 23: Dark I-V characteristic of crystalline photovoltaic cell at halogen lamp illumination of 1000W/m^2.

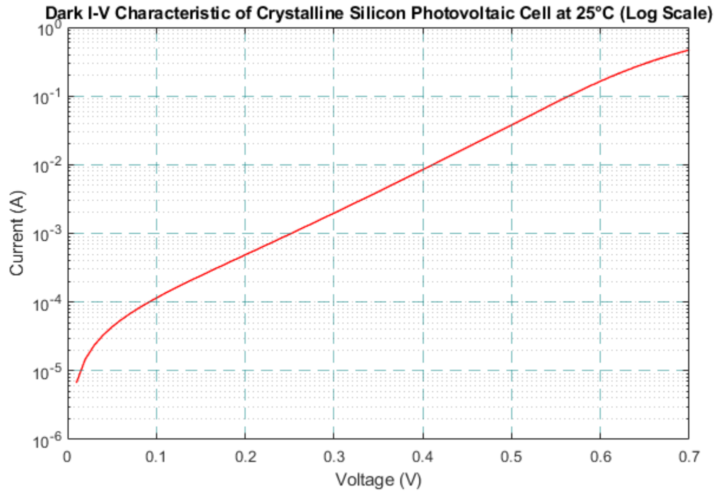

Figure 24: Dark I-V characteristic of crystalline photovoltaic cell with a logarithmic scale.

4.4 SPICE Simulation

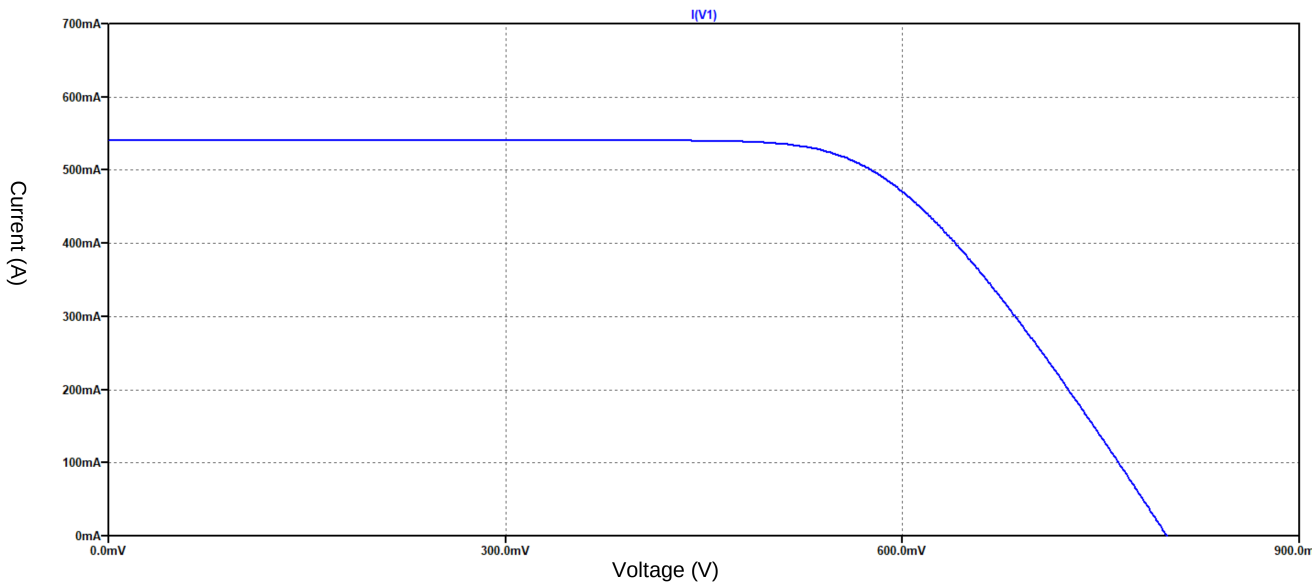

Figure 25: I-V characteristic of simulated 2D two-diode single junction cell.

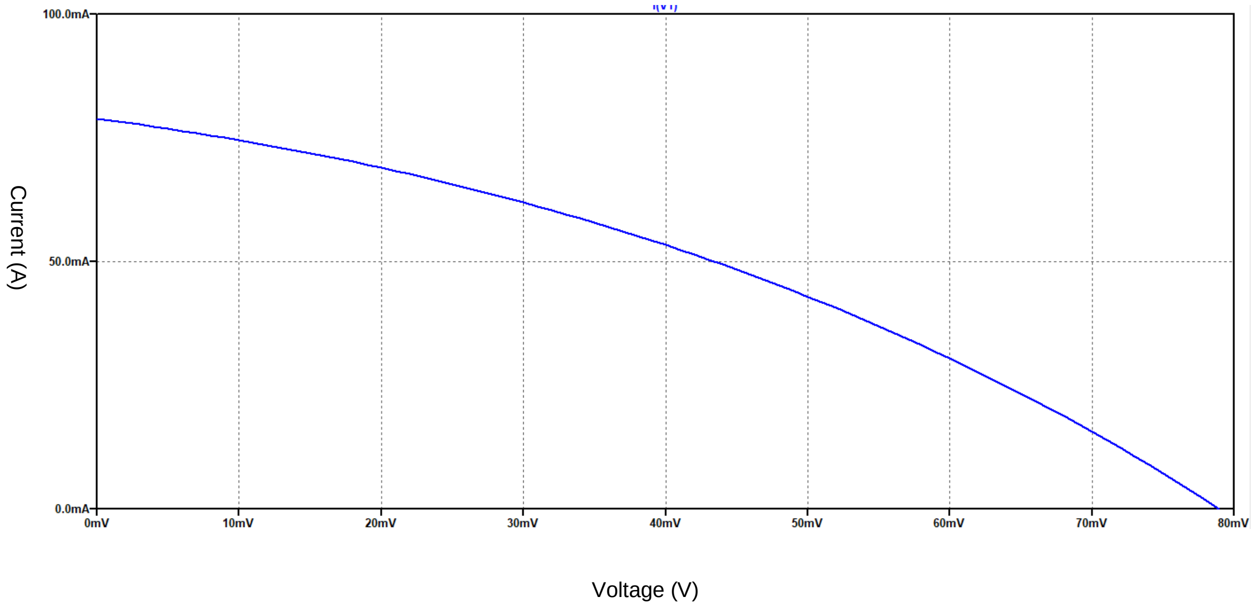

Figure 26: I-V characteristic of simulated 3D single junction cell.

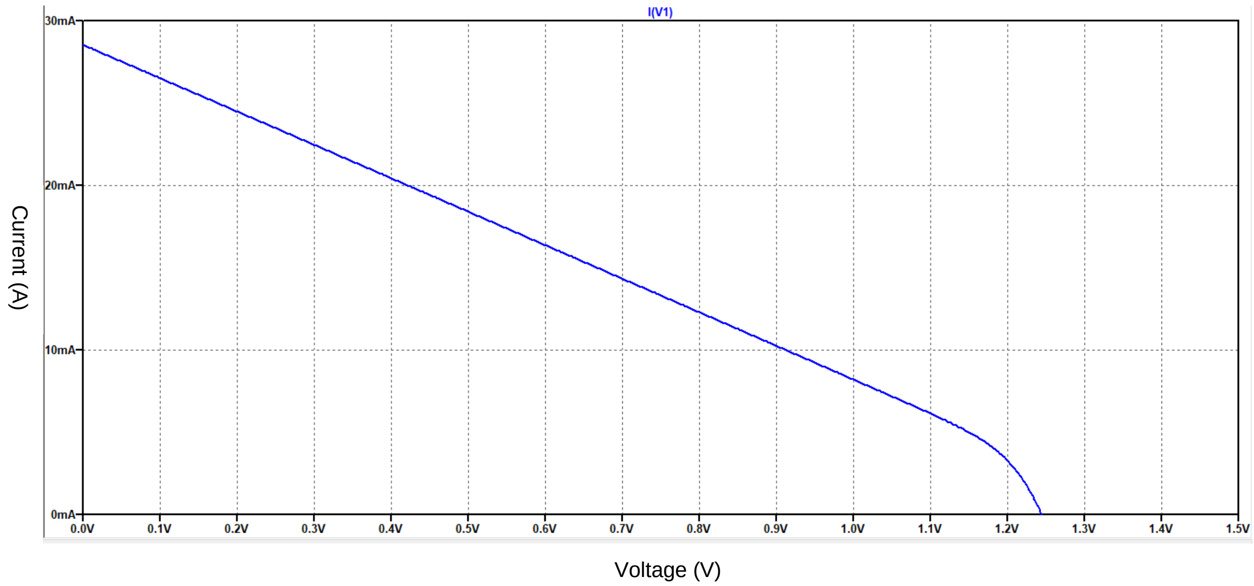

Figure 27: I-V characteristic of simulated 3D triple junction cell.

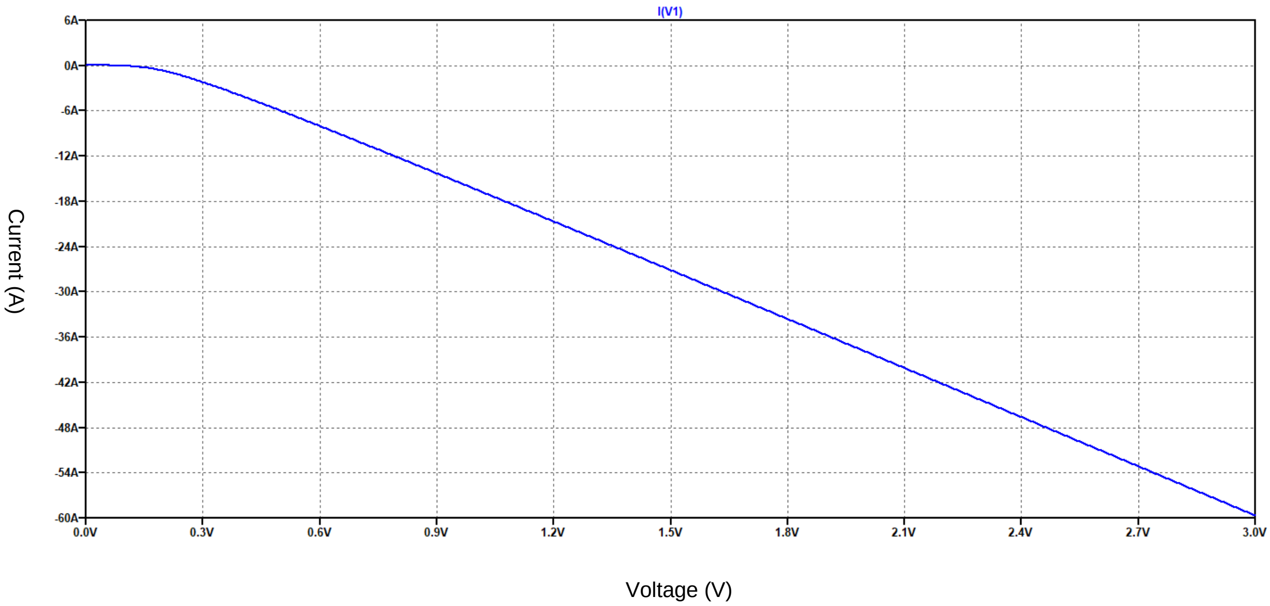

Figure 28: I-V characteristic of simulated 3D single-junction cell (zoomed to fit).

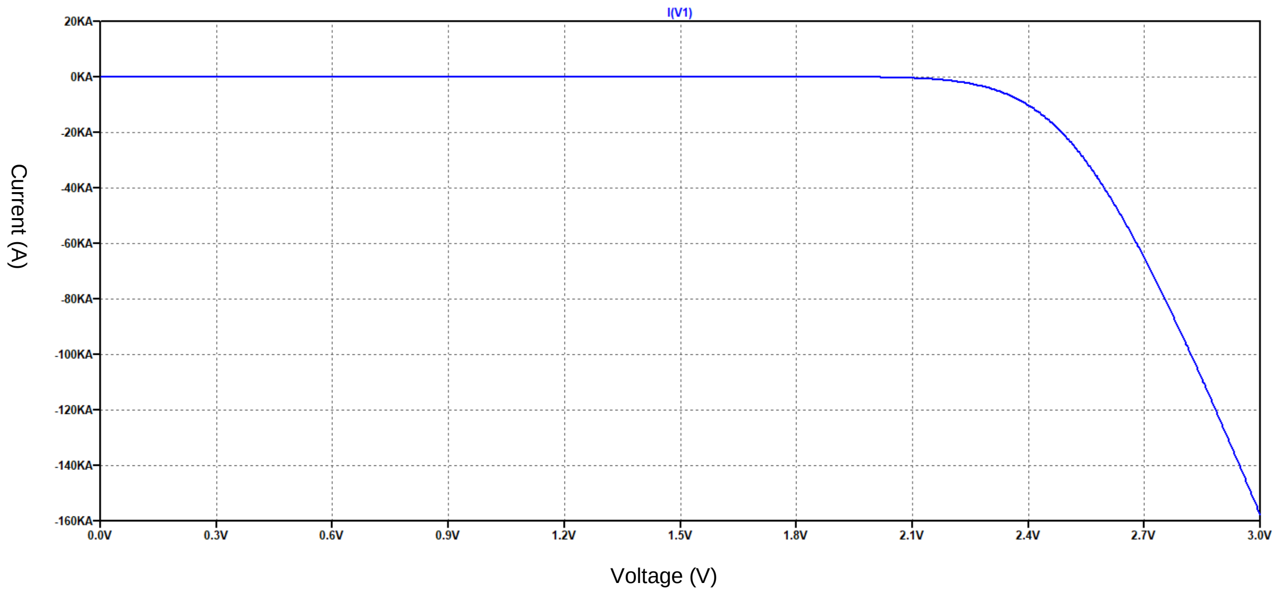

Figure 29: I-V characteristic of simulated 3D triple-junction cell (zoomed to fit).

5. Discussion

5.1 Analysis

5.1.1 I-V Characterisation

As shown in Section 4, the results address two of the objectives stated at the beginning of the report, namely combining two characterisation techniques, I-V characterisation and SPICE simulation. Due to the lack of data, the experimentation serves as a confirmation of accepted techniques within photovoltaic cell research. The I-V characterisation of photovoltaic cells allowed for the extraction of the V_{OC}, I_{SC}, M_{PP}, Fill-factor and efficiency within 13%±1% of the most efficient crystalline silicon cell under halogen illumination and 10%±1% under solar simulation as seen in [56]. For the GaAs cell it was within 9.9%±1% of the most efficient triple-junction photovoltaic cell. These results are a confirmation that the correct methodology was carried out and that the data obtained can be taken as accurate and representative for the type of photovoltaic cell. The I-V characterisation allows for extraction of parameters; however, it does not identify the cause of the losses to the manufacturer or operator of the cell. The only losses that can be identified are the drops in current in the silicon cell which is illuminated with the halogen lamp as it emits a halogen spectrum and as a result has a lower efficiency. This was ideally meant to be addressed by the photoluminescence and electroluminescence imaging to identify the primary loss mechanisms of the multi-junction cells. As a result, the I-V characterisation serves as an effective method for comparison to theoretical values and to analyse the performance of the photovoltaic cell but lacks in analysing the cause of the losses.

5.2 SPICE Simulation

5.2.1 2D Two-diode Model

The curves generated by the models and their corresponding extracted parameters offer little confirmation of experimentally obtained data. Firstly, the 2D two-diode model makes use of arbitrary parameters to produce an I-V characteristic within the general range and shape for a solar cell. The model was produced in order to get a grasp of the software and general behaviour of the production of the characteristic when varying the input parameters. As a conclusion on this model, it can be said that the results are a confirmation of the ability to model the general behaviour of a solar cell using simulation software. The I_{SC} of the simulated diode model was 4.98A±0.01A, V_{OC} was 0.856V±0.01V and the P_{Max} was 3.24W±0.01W. The error for these will also be estimated to be around 1% as they were also digitally obtained from the I-V characteristic in the LTSpice software.

5.2.2 3D Single-junction Model

The production of the 3D model aimed to be a confirmation of the experimentally obtained data. This confirmation would be useful as it would provide an insight into obtaining the maximum theoretical values based on the diode equations with the ability to model losses across the spatially variant material. The simulations would depend on the ideality of the model instead of being affected by physical defects or manufacturing processes. This simulation would allow for the comparison of experimentally obtained data and allow for the specific identification of defects within a 3D model of a solar cell. Manufacturers could use this to improve the process of making the solar cells in order to prevent certain loss mechanisms being present in a physical photovoltaic cell. Furthermore, these loss mechanisms could be reproduced within the simulation to analyse their effect on the performance on the cell.

The production of the model was a cumbersome process which originally stemmed from the difficulty in adjusting the analogue electrical design software to allow for three-dimensional design. Editing the components was not a focus in the research papers, so as a result this is still a point of interest considering it may influence the result. As the shape of the graph is correct and that it is only outside of the range of accepted values, it would appear that the method to produce this is in fact correct but instead the parameters are the cause of the incorrect results. The curves shown in Figure 26 and Figure 27 are zoomed to fit so they show the curve above 0A, however, the shape of the graph for the entire 3V range differs and in Steiner et al., (2012) the curve has a higher current which ranges across the entire 3V and as a result has a larger power produced.

In addition to editing the components, wiring the model came with a lot of difficulty as wiring required previous experience with the software and relied heavily on being able to effectively troubleshoot using the error messages at run-time of the simulation. As error messages are circuit specific and are general messages, finding the solutions to this took a long time. One of the main considerations that needs to be made is avoiding a node being produced when wires cross each other on a plane as this will lead to a simulation that will hang.

Using the parameters in the table presented in Steiner et al., (2012) the values were input into the components and the simulation was run.

The curve produced for the single-junction 3D model is slightly skewed and lies between 0A and -70A. The data extracted is as follows: the simulated cell had an I_{SC} of 0.0196A±0.02mA and a V_{OC} of 0.45V±4.5mV and a P_{Max} of 2.67×10^{-3}W±1mW.

Due to time constraints it was not possible to rectify the results. Nevertheless, it can be seen that the results stem from the parameters entered into the components as initially the simulations were run with the values in the table. It was understood that the values in the table were the absolute values that correspond to each component in the elementary cell. After further analysis, the values are density values that correspond to each component since the model is dependent on the number of elementary cells and the area of the real cell that is being represented. The equations for this are presented earlier in the report and as such, an attempt was made at making these calculations. However, due to limited access to the physical photovoltaic cells it was difficult to obtain measurements for the lengths and widths of the fingers and other parameters outside of research papers. Moreover, the elementary cell equivalent for the dark elementary cells need to be accounted for as they take up a larger area than the width of a finger covers in reality.

5.2.3 3D Triple-junction Model

Making the triple-junction model was almost an identical process, the only difference originating from having one less constituent elementary cell and the presence of tunnel diodes. This model had the same objectives as the single-junction 3D model but aimed to have a greater accuracy as the individual contribution of the individual layers could be accounted for and analysed.

The main issues arose from the tunnel diodes as the values for this were iteratively calculated which significantly increased the difficulty of producing a characteristic, as after several attempts, the simulation would still hang. Steiner et al., (2012) states within the same paper for a triple-junction model that the model can be produced without tunnel diodes and resulted in an I-V curve being generated. Figure 27 shows a curve which is much more characteristic of a solar cell however once again, when looking at the entire curve fit to the graph, it is out of the range by several powers of ten and in the negative range from 0 to -160kA. This points again to the hypothesis that the parameters have not been input correctly. In order to confirm this, the experimentally obtained values for the shunt and series resistance for both the single and triple-junction cell were input into the working one-diode model and the following characteristic was produced. The values extracted were as follows: an I_{SC} of 0.0285A±0.3mA, a V_{OC} of 1.24V±0.01V and a P_{Max} of 0.01W±1x10^{-4}W. Figure 29 shows the curve above 0A but it does not produce a curve for the entire 3V as seen in Figure 30 Steiner et al. (2012) and the P_{Max} is far smaller.

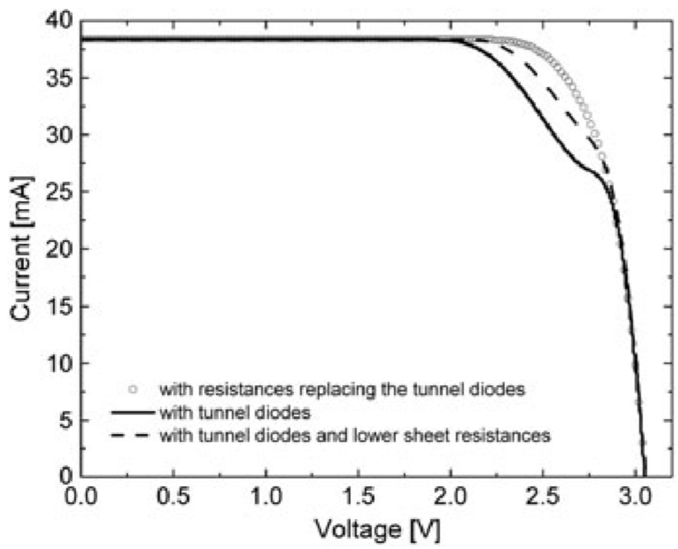

Figure 30: I-V characteristic produced for triple-junction simulation for comparison Steiner et al., (2012).

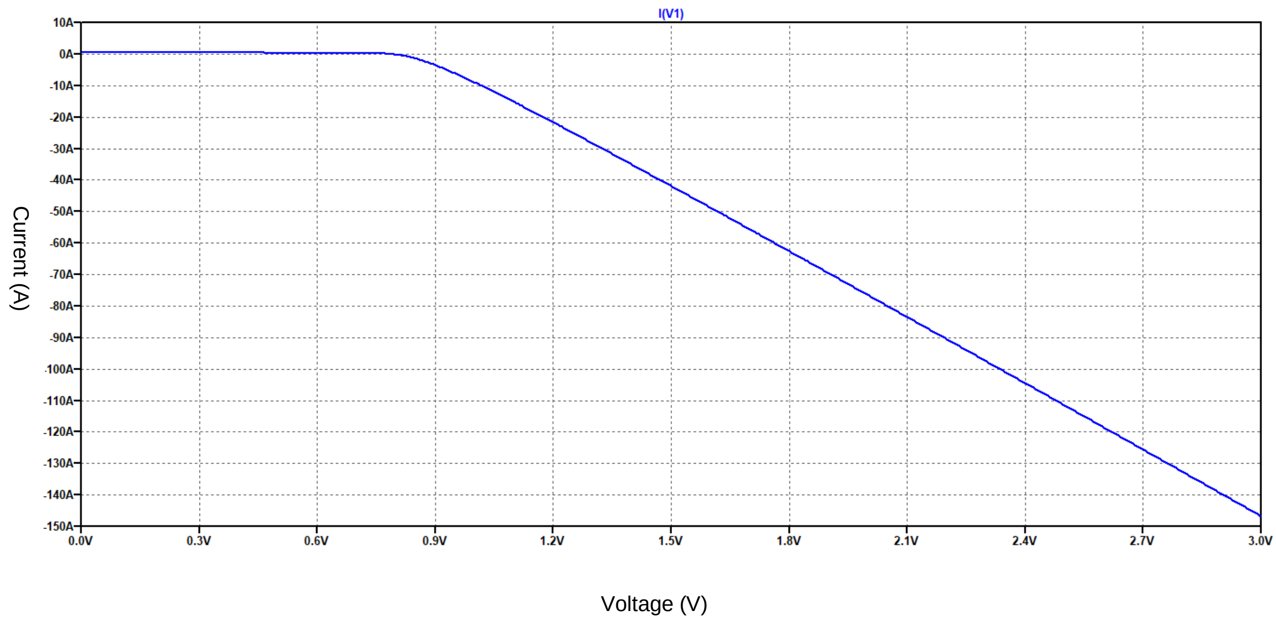

Figure 31: I-V characteristic of two-diode model using experimentally obtained parameters

As seen in the figure above, the I-V curve produced for the one diode model that previously had both the correct shape and range now ranges between 0 and -150A. Although this is a simplification of the issue, it could be a confirmation that both the triple-junction and single-junction 3D model are correct in the simulations but lack the correct parameters.

As an improvement it would've been preferable to make more measurements of the dimensions of the physical cell earlier as this would allow for the calculation of more parameters. This would mean the equations in the papers could be more accurately used and would provide a more accurate representation. Furthermore, it would be advisable to experiment with more variations of parameters and removing lateral resistances between layers.

6. Conclusion

As a summary, the project aimed to produce an extensive characterisation method that would be able to analyse the performance of multi-junction photovoltaic cells and identify loss mechanisms within them. This would be achieved using a combination of I-V characterisation, photoluminescence and electroluminescence imaging with confirmation using SPICE modelling. Due to laboratory inaccessibility it was not possible to obtain the experimental results for the photoluminescence and electroluminescence experimentation as well as producing the I-V characteristics of individual sub-cells in a multi-junction photovoltaic cell. Therefore, the project had to refocus the aims centred around simulation. The objectives were refocused on the use of SPICE modelling to simulate the performance of triple-junction solar cells and model the loss mechanisms through series resistances and shaded areas below the solar cell contacts. To achieve this, I-V characterisation simulation was carried out to validate the model. This has been partially successful and does point to the ability to produce an accurate I-V characteristic with some refinements. The study aimed to be a confirmation of the 3D model of a photovoltaic cell although it could not produce accurate and reproducible results. With more time and access to physical photovoltaic cells in order to obtain dimensional measurements and produce more models, it is possible that an accurate simulation could be demonstrated.

References

[1] Valence band - Energy Education. 2020. Valence band Available at: https://energyeducation.ca/encyclopedia/Valence_band.

[2] Semiconductor Basics – Diode ElectronicsTutorials. 2020. Available at:

https://www.electronics-tutorials.ws/diode/diode_1.html

[3] The P-N Junction | Solid-state Device Theory | Electronics Textbook. 2020. Available at: https://www.allaboutcircuits.com/textbook/semiconductors/chpt-2/the-p-n-junction/.

[4] Challenges of Making Solar Energy Economical > ENGINEERING.com. 2020. Available at: https://www.engineering.com/DesignerEdge/DesignerEdgeArticles/ArticleID/19841/Challenges-of-Making-Solar-Energy-Economical.aspx.

[5] Scott Amyx. 2020. Multi-Junction Photovoltaic Cells. Available at: https://scottamyx.com/2019/05/28/multi-junction-photovoltaic-cells/.

[6] Characteristic Resistance | PVEducation. 2020. Characteristic Resistance | PVEducation. Available at: https://www.pveducation.org/pvcdrom/solar-cell-operation/characteristic-resistance.

[7] Solar Cell Efficiency | PVEducation. 2020. Available at: https://www.pveducation.org/pvcdrom/solar-cell-operation/solar-cell-efficiency. [Accessed 13 May 2020].

[8] Dark IV Measurements | PVEducation. 2020. Dark IV Measurements | PVEducation. Available at: https://www.pveducation.org/pvcdrom/characterisation/dark-iv-measurements.

[9] Photoluminescence Imaging – Metrology – PV-Manufacturing. 2020. Available at:

https://pv-manufacturing.org/metrology/photoluminescence-imaging/

[10] Electroluminescence | PVEducation. 2020. Available at: https://www.pveducation.org/pvcdrom/characterisation/electroluminescence.

[11] Characteristics of Photovoltaic Solar Cells [Analog Devices Wiki]. 2020. Available at: https://wiki.analog.com/university/courses/eps/photovoltaic.

[12] Kaplanis, S. and Kaplani E. (2013). Renewable Energy Systems: Theory, Innovations And Intelligent Applications (renewable Energy Research Development And Policies). Nova Science Pub Inc.

[13] Steiner, M., et al. (2011) Validated front contact grid simulation for GaAs solar cells under concentrated sunlight. Progress in Photovoltaics: Research and Applications, Vol. 19, pp. 73-83

[14] Steiner, M., et al. (2012) A validated SPICE network simulation study on improving tunnel diodes by introducing lateral conduction layers. Progress in Photovoltaics: Research and Applications, Vol. 20, pp. 274-283

[15] SPICE Model ＜What is SPICE?＞ | Electronics Basics | ROHM. 2020. Available at: https://www.rohm.com/electronics-basics/spice/what-is-spice.

[16] Hoex, B., Zhang, W. and Aberle, A. (2012). Advanced Characterisation of Silicon Wafer Solar Cells. *Energy Procedia*, 15, pp.147-154.

[17] Lim, S., Li, J., Steenbergen, E. and Zhang, Y. (2011). Luminescence coupling effects on multijunction solar cell external quantum efficiency measurement. *Progress in Photovoltaics: Research and Applications*, 21(3), pp.344-350.

[18] Nesswetter, H., Lugli, P., Bett, A. and Zimmermann, C. (2013). Electroluminescence and Photoluminescence Characterization of Multijunction Solar Cells. *IEEE Journal of Photovoltaics*, 3(1), pp.353-358.

[19] Seeland, M., Rösch, R. and Hoppe, H. (2011). Luminescence imaging of polymer solar cells: Visualization of progressing degradation. *Journal of Applied Physics*, 109(6), p.064513.

[20] Paire, M. et al., (2011). Measuring sheet resistance of CIGS solar cell's window layer by spatially resolved electroluminescence imaging. *Thin Solid Films*, 519(21), pp.7493-7496.

[21] K. Nishioka et al. (2006). Evaluation of InGaP/InGaAs/Ge triple-junction solar cell and optimization of solar cell’s structure focusing on series resistance for high-efficiency concentrator photovoltaic systems. *Solar Energy Materials & Solar Cells* 90 1308–1321

[22] US EPA. (2019). Global Greenhouse Gas Emissions Data | US EPA. Available at:

https://www.epa.gov/ghgemissions/global-greenhouse-gas-emissions-data

[23] Circuit Globe. 2020. Difference Between Valence Band and Conduction Band (with Comparison Chart) - Circuit Globe. Available at: https://circuitglobe.com/difference-between-valence-band-and-conduction-band.html.

[24] Conduction band - Energy Education. 2020. Available at: https://energyeducation.ca/encyclopedia/Conduction_band.

[25] Fill Factor | PVEducation. 2020. Available at: https://www.pveducation.org/pvcdrom/solar-cell-operation/fill-factor.

[26] Galiana, B., et al. (2005). A 3-D Model for Concentrator Solar Cells Based on Distributed Circuit Units. IEEE Transactions on Electron Devices, Vol. 52(12), pp. 2552-2558.

[27] Zeckry, A. & Al-Mazroo, Y. A. (1996). A Distributed SPICE-Model of a Solar Cell. IEEE Transactions on Electron Devices, Vol. 43(5), pp. 691-700.

[28] Lamorte, F. M. & Abbott, H. D. (1980). Computer Modeling of a Two-Junction, Monolithic Cascade Solar Cell. IEEE Transactions on Electron Devices, Vol. ED-27(1), pp. 231-249.

[29] Luque, A., Sala. G., Abroiro, J. C. (1998). Electric and Thermal Model for non-uniformly illuminated concentration cells. Solar Energy Materials and Solar Cells, Vol. 51, pp. 269-290.

[30] Pieters, E. B. (2011). Spatial Modeling of Thin-Film Solar Modules Using the Network Simulation Method and SPICE [6]

[31] Ho, D. F. & Morgan, D. T. (1991). SPICE Modeling of Cascade Solar Cells. IEEE Proceedings of Southeastcon '91, Vol. 2, pp. 776-780.

[32] Solar Cell Structure | PVEducation. 2020. Available at: https://www.pveducation.org/pvcdrom/solar-cell-operation/solar-cell-structure.

[33] Solar-cell-efficiency enhancement using nanostructures. 2020. Available at: https://spie.org/news/3124-solar-cell-efficiency-enhancement-using-nanostructures?SSO=1.

[34] Chen, S et al. (2015). Thorough subcells diagnosis in a multi-junction solar cell via absolute electroluminescence-efficiency measurements. *Scientific Reports*, 5, 7836.

[35] Carrier recombination and generation. 2019. Available at: https://ecee.colorado.edu/~bart/book/book/chapter2/ch2_8.htm.

[36] ELECTROLUMINESCENCE IMAGING | CEP solar. 2020. Available at: http://www.cepsolar.com/electroluminescence-imaging.

[37] Open-Circuit Voltage | PVEducation. 2019. Available at: https://www.pveducation.org/pvcdrom/solar-cell-operation/open-circuit-voltage.

[38] homogeneous material | JEDEC. 2019. homogeneous material | Available at: https://www.jedec.org/standards-documents/dictionary/terms/homogeneous-material.

[39] Reference. 2020. What Is Forward and Reverse Biasing? | Available at: https://www.reference.com/science/forward-reverse-biasing-c9ff434e6e3c4e4d.

[40] Everything In Science- Physics, Chemistry, Biology and Space. 2020. Available at: https://sciencemonk.com/solar-cell-efficiency/.

[41] Lifetime | PVEducation. 2019. Lifetime | Available at: https://www.pveducation.org/pvcdrom/pn-junctions/lifetime.

[42] Trupke, T et al. 2012. 'Photoluminescence Imaging for Photovoltaic Applications'. *Energy Procedia*. vol. 15. pp. 135-146.

[43] OpenStax CNX. 2020. OpenStax CNX. Available at: https://cnx.org/contents/3QU3ovtd@1/An-Introduction-to-Solar-Cell-Technology.

[44] Advanced multi-junction solar cells deliver high efficiency, reduced costs for space. 2020. Available at: https://phys.org/news/2018-01-advanced-multi-junction-solar-cells-high.html.

[45] Energy.gov. 2020. Multijunction III-V Photovoltaics Research | Department of Energy. Available at: https://www.energy.gov/eere/solar/multijunction-iii-v-photovoltaics-research.

[46] How do Photovoltaics Work? | Science Mission Directorate. 2020. Available at: https://science.nasa.gov/science-news/science-at-nasa/2002/solarcells/.

[47] Alonso-Álvarez, D. et al., (2016). Photoluminescence-Based Current–Voltage Characterization of Individual Subcells in Multijunction. Devices IEEE Journal of Photovoltaics. Vol. 6. Issue. 4

[48] Tsuno, Y. & Hishikawa, Yoshihiro & Kurokawa, Kosuke. (2005). Separation of the I-V curve of each component cell of multi-junction solar cells. Conference Record of the IEEE Photovoltaic Specialists Conference. 1476-1479. 10.1109/PVSC.2005.1488421.

[49] Guter, Wolfgang & Bett, Andreas. (2006). I–V Characterization of Tunnel Diodes and Multijunction Solar Cells. Electron Devices, IEEE Transactions on. 53. 2216 - 2222.

[50] Domínguez C., García-Linares P. (2015) Characterization of Multijunction Concentrator Solar Cells. In: Pérez-Higueras P., Fernández E. (eds) High Concentrator Photovoltaics. Green Energy and Technology. Springer, Cham [3]

[51] S A Kozhukhovskaia et al., (2015) Experimental model of multi-junction solar cell: IV curve tailoring and photoresponce artefact simulation. Journal of Physics: Conference Series 586 012014

[52] Kaltschmitt, K., 2007. Renewable Energy: Technology, Economics And Environment. Springer.

[53] Stephen, P., 2018. Renewable Energy: Power For A Sustainable Future. Oxford University Press.

[54] Trupke, T. et al., (2007). Progress with luminescence imaging for the characterisation of silicon wafers and solar cells. Fraunhofer ISE.

[55] Malik, A. Q. et al., (2010) Influence of Temperature on the performance of Polycrystalline Silicon Module in the Bruneian Climate. ASEAN Journal on Science and Technology for Development Vol. 26, Issue. 2. pp.61-72.

[56] Solar Cell Efficiency Records | PVEducation. 2020. Available at: https://www.pveducation.org/pvcdrom/appendices/solar-cell-efficiency-results2.